

Light induced enhancement of superconductivity via melting of competing bond-density wave order in underdoped cuprates

Aavishkar A. Patel and Andreas Eberlein

Department of Physics, Harvard University, Cambridge MA 02138, USA

(Dated: May 4, 2016)

Abstract

We develop a theory for light-induced superconductivity in underdoped cuprates in which the competing bond-density wave order is suppressed by driving phonons with light. Close to a bond-density wave instability in a system with a small Fermi surface, such as a fractionalized Fermi liquid, we show that the coupling of electrons to phonons is strongly enhanced at the bond-density wave ordering wavevectors, leading to a strong softening of phonons at these wavevectors. For a model of classical phonons with anharmonic couplings, we show that the combination of strong softening and driving can lead to large phonon oscillations. When coupled to a phenomenological model describing the competition between bond-density wave order and superconductivity, these phonon oscillations melt bond-density wave order, thereby enhancing pairing correlations.

arXiv:1602.05964v2 [cond-mat.str-el] 3 May 2016

I. INTRODUCTION

Superconductivity in cuprate materials still poses many questions that lack a theoretical understanding. One is about the maximum value of the critical temperature for superconductivity (T_c) that could be achieved due to the pairing mechanism, which also concerns the effects that limit T_c in practice. Traditionally, the answer to this question was refined by synthesizing new materials or by changing control parameters such as external pressure. A new approach is the manipulation of materials properties such as order parameters by driving phonons with light [1, 2].

In the underdoped regime, T_c is presumably limited by the occurrence of a pseudogap. The nature of this pseudogap state has not yet been clarified, and it is often interpreted as a state with competing orders or preformed pairs. Recent experiments in which the properties of underdoped cuprates are manipulated by driving phonons with light are promising to provide further insights about the physics in the underdoped regime. A series of remarkable experiments reported for example evidence for transient superconducting states induced by light in underdoped Yttrium [3] (YBCO) and Lanthanum [4] (LCO) based cuprates far above T_c , and even up to room temperature in the former case.

In Lanthanum-based cuprates, a transient superconducting state can be induced above T_c around 12% hole doping [4–6], where superconductivity competes strongly with stripe order. In equilibrium and above T_c , stripe order frustrates hopping perpendicular to the copper oxygen layers and destroys interlayer coherence. Stimulation with light leads to a melting of stripe order, which enhances the interlayer coherence and gives rise to a transient superconducting state [7].

The situation for Yttrium based compounds [3] is less clear. From an experimental point of view, there is evidence for the melting of a competing order parameter [8, 9], redistribution of interlayer coupling [9] and non-equilibrium lattice distortions [10, 11]. Evidence also exists for a precursor superconducting state in equilibrium [12]. Several theories try to explain the transient superconducting state as a product of a redistribution of spectral weight [13] or parametric cooling [14] of phase fluctuations due to periodic driving, exploiting the bilayer structure of YBCO. An alternative scenario invokes competition between bond-density wave (BDW) order and superconductivity in a three-dimensional model, where light modulates the interlayer hopping and influences the competition of orders [15].

In the experiments on YBCO, the enhancement of superconductivity is observed when mid-infrared light couples resonantly to infrared phonons [3], which in turn excite Raman phonons via nonlinear couplings [10, 11, 16]. It thus does not seem to be related to a photo-induced redistribution of quasiparticles [17, 18]. The phonon frequencies are mismatched with the plasma resonance and a direct coupling to phase fluctuations seems inefficient. All three above-mentioned theories have difficulties in explaining why BDW correlations melt and pairing correlations appear on roughly the same time scales, while the disappearance of pairing correlations and the reappearance of BDW correlations happens on very different scales [8]. Moreover, the proposed mechanisms either make use of the fact that YBCO is a bilayer cuprate or the electron hopping perpendicular to the copper oxygen layers plays a prominent role.

It is generally believed that the important physics of cuprate superconductors takes place in the copper oxygen planes, with the spacer layers mainly serving as charge reservoirs. It is therefore interesting to ask whether light-induced superconductivity could be achieved in a single copper oxygen plane. This question is intriguing because such a mechanism could also be at work in other cuprate materials that have one or multiple copper oxygen layers per unit cell and where experiments are more difficult.

In this paper we propose a mechanism for light-induced superconductivity based on the competition between BDW correlations and superconductivity, which may be applicable slightly above the equilibrium T_c where the system is close to a BDW instability [19–21]. We describe the interplay of BDW and pairing fluctuations with a phenomenological nonlinear sigma model [22, 23], and investigate the external driving of this model by coupling it to phonons via electrons. Parameter quenches of the non-linear sigma model have been studied by Fu *et al.* in Ref. 24. The electrons are described as a fractionalized Fermi liquid (FL*) [25, 26], which is a model for the pseudogap state in underdoped cuprates. It shows BDW correlations at an axial wave vector that connects the tips of Fermi arcs [27], as seen in experiment [28].

An important ingredient of our theory is the enhanced coupling of electrons and phonons at the BDW wave vector that is observed in experiments. It leads to a strong softening of the phonon dispersion [29, 30] and a phonon linewidth that increases strongly with decreasing temperature [30, 31]. Our theory traces back the enhanced electron-phonon coupling to vertex corrections due to short-range antiferromagnetic fluctuations and explains the phonon

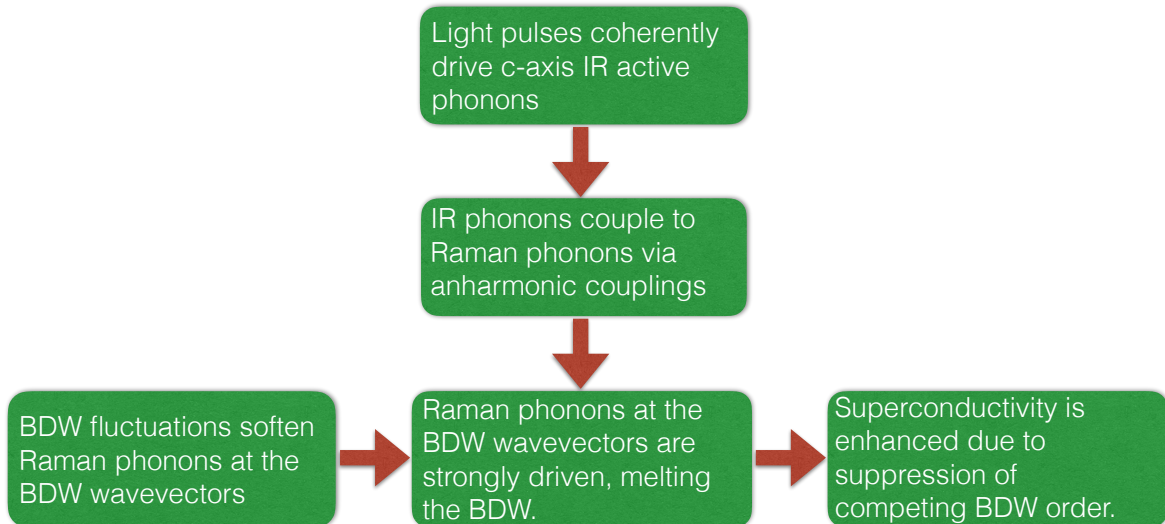


FIG. 1: (Color online) Flow diagram illustrating how the interaction between light, driven phonons, electrons and order parameters can enhance superconductivity.

renormalization above T_c as being a consequence of strong BDW fluctuations. However, the enhanced electron-phonon coupling does not directly lead to an enhancement of T_c because it is restricted to a small region in momentum space and certain non-linear couplings between phonons and pairing fluctuations nearly cancel in our model. Instead, the combination of strong phonon softening and phonon anharmonicities allows for the efficient driving of phonons near the BDW wavevector by light pulses. These strongly driven phonons suppress BDW fluctuations by enhancing their mass, thereby enlarging the relative size of the phase space for pairing, which enhances superconducting correlations.

This paper is organized as follows. In Sec. II, we introduce the effective models for competing BDW and pairing correlations, for electrons in underdoped cuprates (the FL*), their mutual coupling as well as the coupling between electrons and phonons. The most important roles in our theory are played by order parameters and phonons, whereas the electrons only act as intermediaries between them. In Sec. III, we introduce a model for driven phonons and describe its renormalization by interaction effects as well as its dynamics close to a BDW instability. We find strong phonon softening that can entail momentum-selective driving and large amplitudes at the BDW wave vector. In Sec. IV, we derive effective couplings between phonons, BDW and pairing fluctuations and describe how the driving of phonons impacts the interplay between BDW and pairing fluctuations. Large phonon amplitudes at the BDW wave vector can lead to a suppression of BDW correlations

in favor of superconductivity. This interplay is summarized in Fig. 1. In Sec. V we discuss our results and draw conclusions.

II. MODEL

We are interested in the temperature region above the critical temperature for superconductivity T_c , where YBCO shows strong bond-density wave fluctuations [19]. In this regime, the interplay between superconducting and bond-density wave fluctuations can be described by a Landau theory of competing orders. In order to minimize the number of couplings in such a theory we choose to use a classical non-linear sigma model (NLSM) that correctly captures various qualitative features of the behavior of competing orders in the pseudogap phase slightly above T_c [22, 23],

$$\mathcal{Z}_{\text{cl}} = \int \mathcal{D}\Psi \mathcal{D}\Psi^* \prod_{n=x,y} \mathcal{D}\Phi_n \mathcal{D}\Phi_n^* e^{-\beta S_{\text{cl}}} \delta(|\Psi|^2 + \sum_{n=x,y} |\Phi_n|^2 - 1), \quad (1)$$

$$S_{\text{cl}} = \rho_s \int d^2\mathbf{x} \left[\frac{1}{2} |\nabla\Psi|^2 + \sum_{n=x,y} \left(\frac{\eta}{2} |\nabla\Phi_n|^2 + \frac{m^2}{2} |\Phi_n|^2 \right) \right], \quad (2)$$

where Ψ and Φ_n are complex bosonic fields describing pairing and BDW fluctuations, respectively. They are combined into an $O(6)$ order parameter with fixed length in order to focus on angular fluctuations. At the lowest temperatures, superconductivity is favored due to the positive mass term for BDW fluctuations. As T is increased, superconducting order is lost, which is aided by the strengthening of BDW fluctuations. As will become clear in the following sections, our mechanism does not specifically require this model and will work for a generic Landau theory of competing orders, since it relies only on the discrepancies in mass renormalizations of different order parameters.

We derive the coupling of the non-linear sigma model to phonons from a phenomenological model for electrons in underdoped cuprates, which we take as a fractionalized Fermi liquid (FL*) [25, 26]. In this model, the Fermi surface is gapped out in the anti-nodal region of the Brillouin zone and reconstructed into hole-like pockets with low spectral weight on their back-sides. It shows incommensurate BDW fluctuations that are peaked at axial wave vectors close to those seen in experiment [27, 32, 33]. The model is defined by the action

$$\mathcal{L}_{\text{f}} = \sum_{k,\sigma} \psi_{\sigma}^{\dagger}(k) G^{-1}(k) \psi_{\sigma}(k) + \mathcal{L}_{\text{int,f}} + \mathcal{L}_{\text{f-BDW}} + \mathcal{L}_{\text{f-dSC}} + \mathcal{L}_{\text{f-ph}} \quad (3)$$

where $\psi^{(\dagger)}$ are fermionic Grassmann fields, $k = (\omega_n, \mathbf{k})$ collects Matsubara frequencies ω_n and momenta \mathbf{k} , $\sigma = \uparrow, \downarrow$ and G^{-1} is the inverse electron propagator. $\mathcal{L}_{\text{int},f}$ describes short-range electron-electron interactions. The other terms couple electrons to BDW fluctuations, d -wave pairing fluctuations and phonons, respectively, and are detailed below. The electron propagator is given by

$$G(k) = \frac{Z}{i\omega_n - \xi_{\mathbf{k}}^+ - \Sigma(k)} \quad (4)$$

where

$$\xi_{\mathbf{k}}^+ = \varepsilon_{\mathbf{k}} + \tilde{\varepsilon}_{\mathbf{k}}, \quad \xi_{\mathbf{k}}^- = \varepsilon_{\mathbf{k}} - \tilde{\varepsilon}_{\mathbf{k}}, \quad (5)$$

$$\varepsilon_{\mathbf{k}} = -2t_1(\cos k_x + \cos k_y) - 4t_2 \cos k_x \cos k_y - 2t_3(\cos(2k_x) + \cos(2k_y)) - \mu, \quad (6)$$

$$\tilde{\varepsilon}_{\mathbf{k}} = -\tilde{t}_0 - \tilde{t}_1(\cos k_x + \cos k_y) \quad (7)$$

is the electron dispersion,

$$\Sigma(k) = \frac{\lambda^2}{i\omega_n - \xi_{\mathbf{k}+\mathbf{K}}^-} \quad (8)$$

the self-energy of the FL* and $\mathbf{K} = (\pi, \pi)$. The hopping parameters used in this work are listed in the caption of Fig. 2. The Fermi liquid form of the propagator in Eq. (4) is manifest if it is rewritten in the following “two-band” form,

$$G(k) = \sum_{\alpha=\pm} \frac{Z_{\mathbf{k}}^{\alpha}}{i\omega_n - E_{\mathbf{k}}^{\alpha}}, \quad Z_{\mathbf{k}}^{\alpha} = \frac{Z^2(E_{\mathbf{k}}^{\alpha} - \xi_{\mathbf{k}+\mathbf{K}}^-)^2}{\lambda^2 + (E_{\mathbf{k}}^{\alpha} - \xi_{\mathbf{k}+\mathbf{K}}^-)^2}, \quad (9)$$

$$E_{\mathbf{k}}^{\pm} = \frac{1}{2}(\xi_{\mathbf{k}}^+ + \xi_{\mathbf{k}+\mathbf{K}}^-) \pm \sqrt{\lambda^2 + \frac{1}{4}(\xi_{\mathbf{k}}^+ - \xi_{\mathbf{k}+\mathbf{K}}^-)^2}. \quad (10)$$

The gap parameter λ arises from short-range antiferromagnetic order [32] and leads to the reconstruction of the Fermi surface. The parameters \tilde{t}_0 and \tilde{t}_1 control the location of the hole pockets. For $\lambda \neq 0$ but $\tilde{t}_0 = \tilde{t}_1 = 0$, they are centered at $(\pm\pi/2, \pm\pi/2)$. Setting these FL* parameters to zero, we recover the “large Fermi surface”. Examples for a large and small Fermi surface are shown in Fig. 2. We will also comment on the impact of using a small vs. a large Fermi surface on our theory. The parameter Z measures the weight of the fermionic quasiparticles relative to that of incoherent excitations and is not important for our purposes. We thus set $Z = 1$.

We take into account nearest-neighbor exchange interactions,

$$\mathcal{L}_{\text{int},f} = \sum_{k,k',q,\sigma_i} J(\mathbf{q}) \boldsymbol{\tau}_{\sigma_1\sigma_4} \cdot \boldsymbol{\tau}_{\sigma_2\sigma_3} \psi_{k+q/2,\sigma_1}^{\dagger} \psi_{k'-q/2,\sigma_2}^{\dagger} \psi_{k'+q/2,\sigma_3} \psi_{k-q/2,\sigma_4}, \quad (11)$$

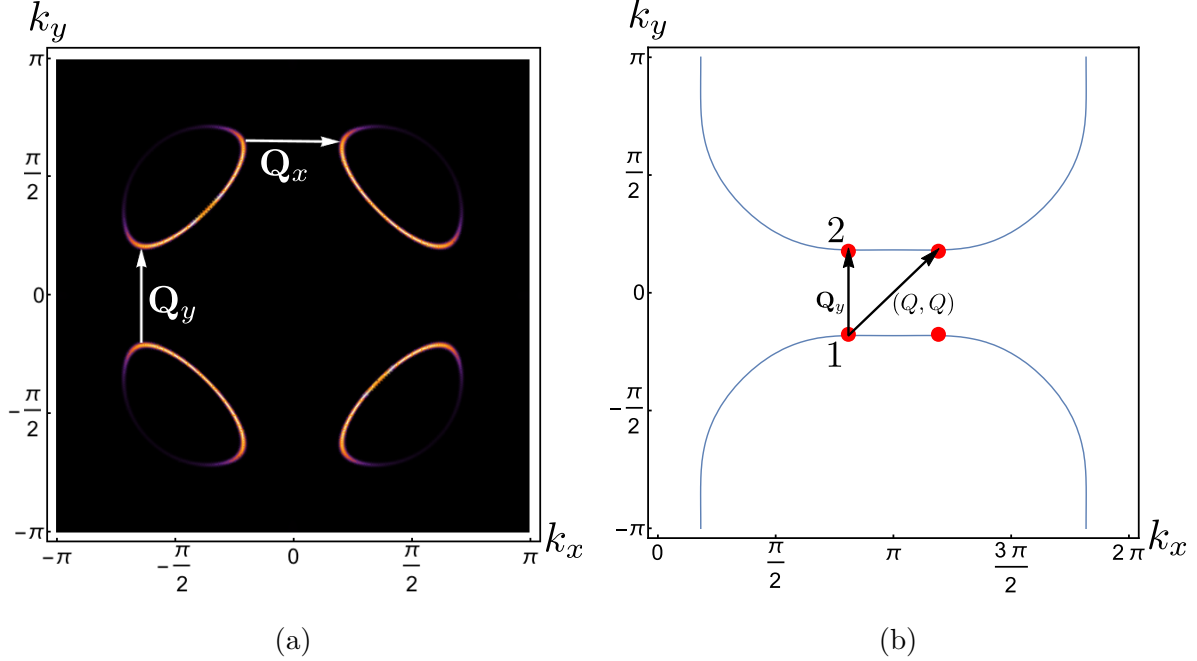


FIG. 2: (Color online) Comparison between (a) small and (b) large Fermi surfaces. Also shown are possible BDW ordering wave vectors. These connect the tips of the hole pockets in (a) or the antiferromagnetic hot spots (marked in red) in (b). In (a) we show the spectral function at $\omega = 0$ with color encoding spectral weight. For this figure, and for the rest of this work, we use $t_1 = 1.0$, $t_2 = -0.32$, $t_3 = 0.128$, $\mu = -1.119$, $\tilde{t}_0 = -0.5t_1$, $\tilde{t}_1 = 0.4t_1$, $\lambda = 0.6t_1$.

where $J(\mathbf{q}) = 2J(\cos q_x + \cos q_y)$, in order to mimic the strong short-range antiferromagnetic correlations that are found in underdoped cuprates. These can induce BDW instabilities [27] of the FL*. For simplicity we restrict ourselves to nearest-neighbor exchange. Further neighbor and density-density interactions could be added, but are not expected to change our results in an essential way.

In order to study the interaction between phonons and pairing as well as BDW fluctuations, we introduce fermion-boson couplings. The coupling of electrons to BDW fluctuations and Cooper pairs could be derived from Hubbard-Stratonovich transformations of short-range interactions. For simplicity, we use phenomenological expressions and couple BDW

fluctuations and electrons via [27, 34]

$$\mathcal{L}_{\text{f-BDW}} = \lambda_{\text{BDW}} \sum_{k,q,n=\{x,y\},\sigma} g_{\mathbf{Q}_n}(k) \psi_{k+\mathbf{Q}_n/2+q/2,\sigma}^\dagger \psi_{k-\mathbf{Q}_n/2-q/2,\sigma} \Phi_n(q) + \text{c.c.}, \quad (12)$$

where λ_{BDW} is the coupling strength and $n = \{x, y\}$ sums over the wavevectors at which the BDW fluctuations are strongest, $\mathbf{Q}_x = (\pm q, 0)$ and $\mathbf{Q}_y = (0, \pm q)$. The intra-unit cell structure of the BDW fluctuations has predominantly d -wave character [27, 35–37]. We therefore approximate the form factor $g_{\mathbf{Q}_n}(\mathbf{k})$ by

$$g_{\mathbf{Q}_n}(\mathbf{k}) \approx g_d(\mathbf{k}) = \cos k_x - \cos k_y \quad (13)$$

and neglect possible admixtures with s -wave symmetry for simplicity. d -wave pairing fluctuations couple to the electrons as

$$\mathcal{L}_{\text{f-dSC}} = \lambda_{\text{dSC}} \sum_{\mathbf{k},\mathbf{q},\sigma} g_d(\mathbf{k}) \psi_{q/2+k,\uparrow}^\dagger \psi_{q/2-k,\downarrow}^\dagger \Psi(q) + \text{c.c.}, \quad (14)$$

where λ_{dSC} is the coupling constant. The value of the coupling constants λ_{BDW} and λ_{dSC} is not important and expected to be of $\mathcal{O}(1)$.

The coupling of electrons to phonons, which are described by real scalar fields φ , is modeled by

$$\mathcal{L}_{\text{f-ph}} = \lambda_{\text{ph}} \sum_{k,q,\sigma} g_{\text{ph}}(\mathbf{q}, \mathbf{k}) \psi_{k+q/2,\sigma}^\dagger \psi_{k-q/2,\sigma} \varphi(q) + \text{c.c.} . \quad (15)$$

In the following we consider the coupling of electrons to buckling modes of the Copper oxygen plane, for which we can generically consider $g_{\text{ph}}(\mathbf{q}, \mathbf{k}) = g_{\text{ph}}(\mathbf{q})$, with [38]

$$|g_{\text{ph}}(\mathbf{q})|^2 = \cos^2\left(\frac{q_x}{2}\right) + \cos^2\left(\frac{q_y}{2}\right). \quad (16)$$

The dependence on \mathbf{q} is not very important and our conclusions do not change in case a momentum independent bare vertex, $g_{\text{ph}}(\mathbf{q}) = g_{\text{ph}}$, is used. In the next section, we will see that strong fluctuations at an incipient BDW instability will induce a \mathbf{k} dependence for the electron-phonon vertex. The action describing the phonon dynamics is also detailed in the next section.

III. PHONON RENORMALIZATION AND PHONON DYNAMICS NEAR BOND-DENSITY WAVE INSTABILITY

In the experiments on YBCO [3], the laser pulses drive c -axis infrared (IR) phonons. Since the pulse wavelength is much larger than the lattice constants, the IR phonons can be

considered to be excited at zero momentum. The IR phonons then couple to the in-plane Raman phonons, which in turn couple to the electrons [16, 39]. We model the dynamics of the Raman phonons with the classical real-time Lagrangian with quartic anharmonicities developed by Subedi *et al.* for cuprate superconductors [16],

$$\mathcal{L}_{\text{ph}} = \int d^2\mathbf{x} \frac{1}{2}(\partial_t\varphi(\mathbf{x}))^2 - \frac{1}{2}\omega_{\text{ph},0}^2\varphi(\mathbf{x})^2 + \frac{r}{2}\phi_{\text{IR}}(\mathbf{x})^2\varphi(\mathbf{x})^2 - \frac{u}{4}\varphi(\mathbf{x})^4, \quad (17)$$

where $\omega_{\text{ph},0}$ is the bare Raman phonon frequency. The dispersion of the (optical) Raman phonons is mostly flat throughout the Brillouin zone, so we do not include gradient terms in the Lagrangian. $\phi_{\text{IR}}(\mathbf{x}) \sim A_{\text{IR}} \cos(\omega t)$ is the amplitude of the driven IR phonon and r the coupling between (odd under inversion) IR and (even under inversion) Raman phonons. Since the Lagrangian must be inversion symmetric, the Raman phonons must couple to ϕ_{IR}^2 instead of ϕ_{IR} at lowest order. The anharmonic coupling $u > 0$ is important in order to stabilize the strongly driven system. Note that the IR phonon does not possess any dynamics besides the driving and that all phonons are described as classical oscillators. This is justifiable for the strongly driven phonons in the experiments, where the phonon amplitudes reach a few percent of the lattice constants [10, 11].

Before studying the phonon dynamics described by the action in Eq. (17), we compute the phonon renormalization near a BDW instability. In such a situation, a strong renormalization of phonons has been observed in x-ray scattering experiments [30, 31]. In the experiment by Le Tacon *et al.* [30], a significant softening of the dispersion of IR phonons together with a strongly increased linewidth is observed at the BDW wave vector. As described by our model below, this effect should carry over to Raman phonons as well.

Intuitively, we expect that the short-range antiferromagnetic fluctuations that drive the BDW instability at a particular wavevector can also significantly renormalize the electron-phonon vertex at that wavevector. We thus consider the renormalization of this vertex by short-range antiferromagnetic fluctuations close to a BDW instability via a Bethe-Salpeter equation. Assuming the electron-phonon vertex to be independent of frequency and spin, the renormalized electron-phonon term is given by

$$\mathcal{L}_{\text{e-ph}} = \sum_{k,\mathbf{q},\sigma=\uparrow,\downarrow} \Gamma(\mathbf{q},\mathbf{k})\psi_{k+\mathbf{q}/2,\sigma}^\dagger\psi_{k-\mathbf{q}/2,\sigma}\varphi(\mathbf{q}) + \text{H.c.} \quad (18)$$

where the bare vertex $\Gamma_0(\mathbf{q},\mathbf{k}) = \lambda_{\text{ph}}g_{\text{ph}}(\mathbf{q})$. For simplicity we expand the dependence on

ℓ	Basis Function $f_\ell(\mathbf{k})$
0	1
1	$\cos(k_x) + \cos(k_y)$
2	$\cos(k_x) - \cos(k_y)$
3	$\sin(k_x) + \sin(k_y)$
4	$\sin(k_x) - \sin(k_y)$

TABLE I: Basis functions for decomposing the renormalized electron-phonon vertex

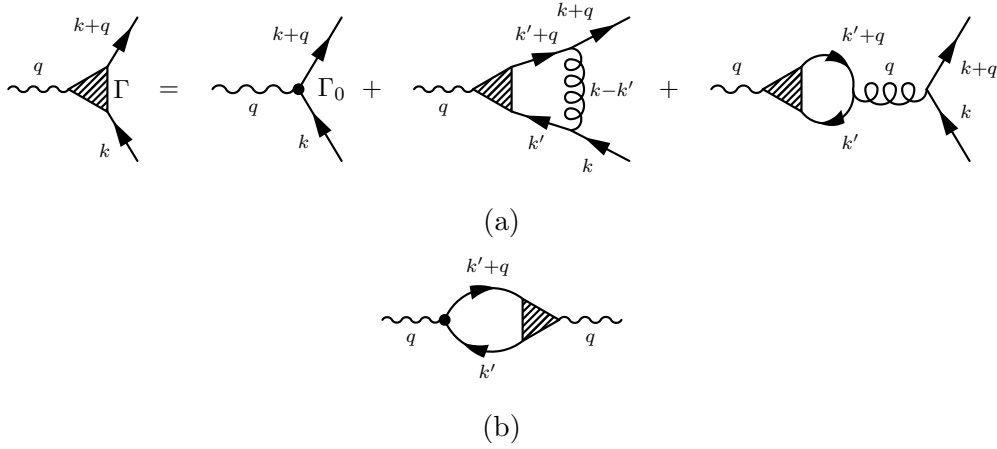


FIG. 3: Diagrammatic representation of (a) the Bethe-Salpeter equation for the electron-phonon vertex and (b) the phonon self-energy.

electron momenta \mathbf{k} using basis functions,

$$\Gamma(\mathbf{q}, \mathbf{k}) = \sum_{\ell=0}^4 \Gamma_\ell(\mathbf{q}) f_\ell(\mathbf{k}), \quad (19)$$

which are chosen keeping in mind the nearest-neighbor nature of the short range anti-ferromagnetic fluctuations and are given in Table I. The Bethe-Salpeter equation for the electron-phonon vertex is diagrammatically depicted in Fig. 3a and reads

$$\Gamma_j(\mathbf{q}) = \delta_{j0} \lambda_{\text{ph}} g_{\text{ph}}(\mathbf{q}) - \sum_{\ell=0}^4 \Gamma_\ell(\mathbf{q}) M_{j\ell}(\mathbf{q}), \quad (20)$$

$$M_{j\ell}(\mathbf{q}) = (1 - \delta_{j0}) \frac{3J}{2} \int \frac{d^2 \mathbf{k}'}{(2\pi)^2} \Pi(\mathbf{k}', \mathbf{q}) f_j(\mathbf{k}') f_\ell(\mathbf{k}'), \quad (21)$$

$$\Pi(\mathbf{k}', \mathbf{q}) = \sum_{\alpha_1, \alpha_2 = \pm} Z_{\mathbf{k}'+\mathbf{q}/2}^{\alpha_1} Z_{\mathbf{k}'-\mathbf{q}/2}^{\alpha_2} \frac{n_f(E_{\mathbf{k}'+\mathbf{q}/2}^{\alpha_1}) - n_f(E_{\mathbf{k}'-\mathbf{q}/2}^{\alpha_2})}{E_{\mathbf{k}'+\mathbf{q}/2}^{\alpha_1} - E_{\mathbf{k}'-\mathbf{q}/2}^{\alpha_2}}. \quad (22)$$

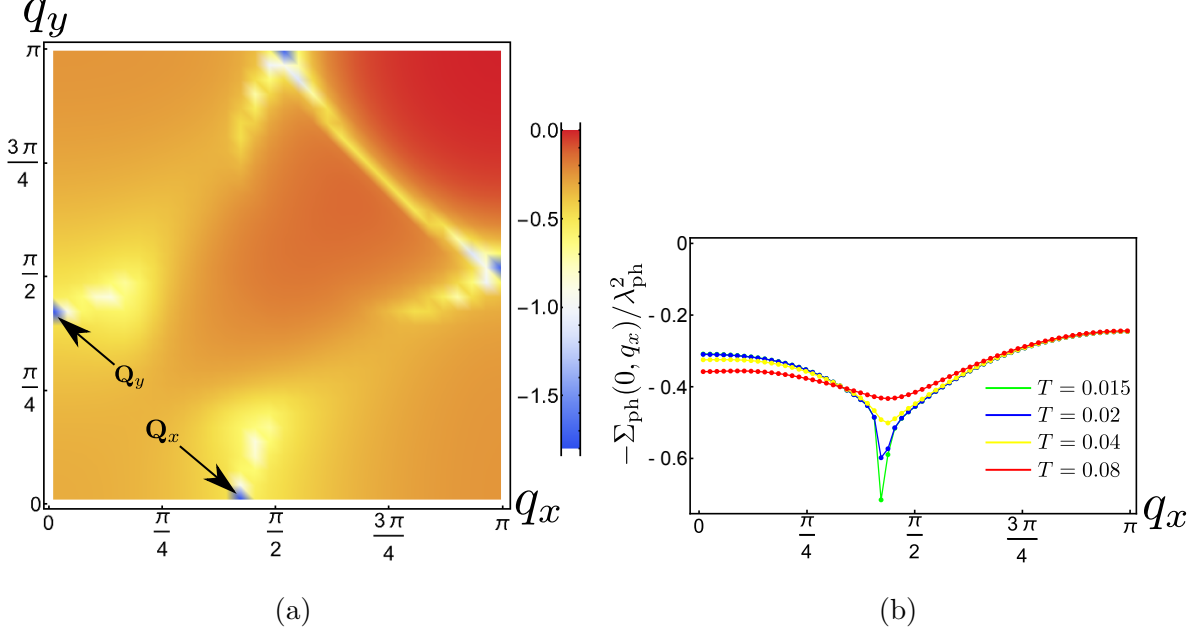


FIG. 4: (Color online) (a) Phonon self-energy $-\Sigma_{\text{ph}}(0, \mathbf{q})/\lambda_{\text{ph}}^2$ as a function of \mathbf{q} for $J = 2.07$ and $T = 0.01$. The strongest softening occurs at the BDW wavevectors \mathbf{Q}_x and \mathbf{Q}_y which are marked in the figure. (b) Cuts along the q_x axis of (a) for several temperatures. At $T = 0.01$, the system is very close to the BDW instability for the value of J chosen.

The antiferromagnetic interaction does not renormalize the s -wave component of the vertex. This can be achieved by adding density-density interactions. It is also possible to add further neighbor couplings. These should, however, not impact our conclusions in an essential way.

The renormalized phonon dispersion $\omega_{\text{ph}}(\mathbf{q})$ is given by

$$\omega_{\text{ph}}^2(\mathbf{q}) = \omega_{\text{ph},0}^2 - \Sigma_{\text{ph}}(0, \mathbf{q}) \quad (23)$$

where

$$\Sigma_{\text{ph}}(0, \mathbf{q}) = -\lambda_{\text{ph}} g_{\text{ph}}(\mathbf{q}) \int \frac{d^2 \mathbf{k}'}{(2\pi)^2} \Gamma(\mathbf{q}, \mathbf{k}') \Pi(\mathbf{k}', \mathbf{q}) \quad (24)$$

is the static phonon self-energy computed with the renormalized electron-phonon vertex, as depicted in Fig. 3b. Close to a BDW instability, we obtain a significant softening of the phonon modes at wavevectors near \mathbf{Q}_n , as shown in Fig. 4. The softening gets more pronounced with decreasing temperature and/or increasing antiferromagnetic interaction J . A similar Bethe-Salpeter equation for the electron-BDW fluctuation vertex λ_{BDW} yields a strong enhancement of λ_{BDW} close to the BDW instability.

Once T is low enough, the system becomes superconducting and the above analysis no longer applies. It thus cannot explain by itself the jump in phonon softening at T_c noted in Ref. 30. However, it would be interesting to repeat their experiment in the presence of a magnetic field that suppresses superconductivity, in which case we would expect a stronger phonon softening with decreasing temperature and increasing BDW correlation length.

We now study the phonon dynamics described by Eq. (17), where $\omega_{\text{ph},0}$ is replaced by the renormalized phonon frequency $\omega_{\text{ph}}(\mathbf{q})$. Since the dispersion minima now lie effectively at \mathbf{Q}_n , we write down the effective Lagrangian for these modes consistent with translation, inversion and C_4 rotation symmetry

$$\begin{aligned} \mathcal{L}_{\text{ph,eff}} = \int d^2\mathbf{x} \left[\sum_{n=\{x,y\}} \left((\partial_t \varphi(\mathbf{Q}_n))^2 - K^2 |\nabla \varphi(\mathbf{Q}_n)|^2 \right. \right. \\ \left. \left. - (\omega_{\text{ph}}(\mathbf{Q}_n)^2 - r A_{\text{IR}} \cos^2(\omega t)) |\varphi(\mathbf{Q}_n)|^2 - \frac{u}{4} |\varphi(\mathbf{Q}_n)|^4 \right) - u' |\varphi(\mathbf{Q}_x)|^2 |\varphi(\mathbf{Q}_y)|^2 \right]. \end{aligned} \quad (25)$$

From this, we obtain the equations of motion of the fundamental modes

$$\begin{aligned} \partial_t^2 \varphi(\mathbf{Q}_x) + (\omega_{\text{ph}}^2(\mathbf{Q}_x) - r A_{\text{IR}}^2 \cos^2(\omega t)) \varphi(\mathbf{Q}_x) \\ + \frac{u}{2} \varphi(\mathbf{Q}_x)^2 \varphi^*(\mathbf{Q}_x) + u' \varphi(\mathbf{Q}_x) |\varphi(\mathbf{Q}_y)|^2 + \gamma(\mathbf{Q}_x) \partial_t \varphi(\mathbf{Q}_x) = 0, \end{aligned} \quad (26)$$

and the partner equations for $x \leftrightarrow y$ and $\varphi \leftrightarrow \varphi^*$, where we also added Landau damping terms representing effects of the imaginary part of the phonon self-energy, which we have not computed explicitly. This Landau damping will be enhanced by the large value of $\Gamma(\mathbf{Q}_n, \mathbf{k})$ close to the BDW instability, leading to spectral broadening at those wavevectors, as seen in experiments. For simplicity in illustrating qualitative features, we consider C_4 symmetric initial conditions with real mode values and $u' = u/2$. The equations then read

$$\partial_t^2 \varphi(\mathbf{Q}_n) + (\omega_{\text{ph}}^2(\mathbf{Q}_n) - r A_{\text{IR}}^2 \cos^2(\omega t)) \varphi(\mathbf{Q}_n) + u \varphi(\mathbf{Q}_n)^3 + \gamma(\mathbf{Q}_n) \partial_t \varphi(\mathbf{Q}_n) = 0. \quad (27)$$

These equations exhibit the well known Mathieu instability [16, 40, 41] for large enough driving amplitudes, when the control parameter ν exceeds a critical value,

$$\nu = \frac{r A_{\text{IR}}^2}{2 \omega_{\text{ph}}^2(\mathbf{Q}_n)} > \nu_c = 1 + \frac{\omega_{\text{ph}}^2(\mathbf{Q}_n)}{8 \omega^2} + \dots \quad (28)$$

The instability happens first for the softened phonons for $r > 0$. The anharmonic coupling $u > 0$ stabilizes the system and allows the phonon potential to acquire a double well shape.

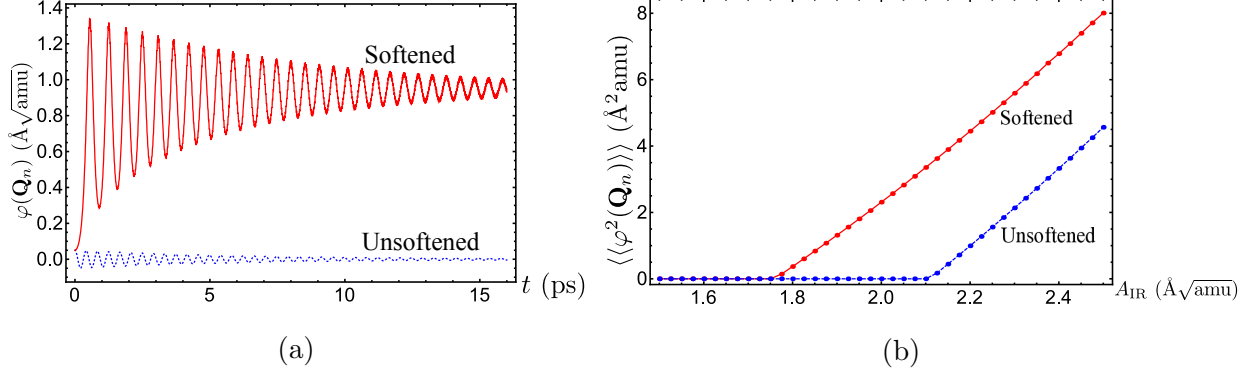


FIG. 5: (Color online) (a) Phonon dynamics for unsoftened phonons with $\nu < \nu_c$ (dashed, blue) and for softened phonons with $\nu > \nu_c$ (solid, red). We use parameters from Ref. 16, a softening of $\sim 15\%$ and a small damping: The phonon frequencies are $\omega_{\text{ph}}(\mathbf{Q}_n)^2 = 103.55 \text{ meV}/\text{\AA}^2/\text{amu} = \omega_{\text{ph},0}^2$ for the unsoftened phonon (dashed, blue) and $\omega_{\text{ph}}^2(\mathbf{Q}_n) = 72.55 \text{ meV}/\text{\AA}^2/\text{amu}$ for the softened phonon (solid, red) and other parameters are $\omega^2 = 1462.3 \text{ meV}/\text{\AA}^2/\text{amu}$, $r = 46.98 \text{ meV}/\text{\AA}^4/\text{amu}^2$, $u = 8.36 \text{ meV}/\text{\AA}^4/\text{amu}^2$, $\gamma^2(\mathbf{Q}_n) = 0.01 \text{ meV}/\text{\AA}^2/\text{amu}$ and $A_{\text{IR}} = 1.85 \text{\AA}\sqrt{\text{amu}}$. The value of the softening used corresponds to an energy difference of about 3 meV. (b) The mean-square amplitude of the phonons as a function of the driving amplitude A_{IR} .

The phonons then oscillate about the minima of the double well instead of about zero, and the damping terms simply damp out these oscillations (see Fig. 5a). In this regime, an average displacement of the Raman mode is possible. Equation (27) also shows an instability for $r < 0$ [41], but in this case it does not happen first for the softest phonons and the physics is different.

Figure 5 shows examples for the phonon dynamics in different regimes, highlighting the impact of phonon softening. The parameters used in this figure are taken from Ref. 16. Since ν increases when $\omega_{\text{ph}}(\mathbf{Q}_n)$ is softened, it is possible that a significant softening for Raman phonons close to the BDW instability can lead to the modes near \mathbf{Q}_n being in the $\nu > \nu_c$ regime, thereby acquiring large oscillation amplitudes. Equivalently, if A_{IR} is large enough, these modes will enter this regime. Thus, phonon anharmonicities in combination with momentum-specific phonon softening can lead to a strong driving of Raman modes close to the BDW ordering wavevectors. The dynamics of phonon modes at momenta away from \mathbf{Q}_n ,

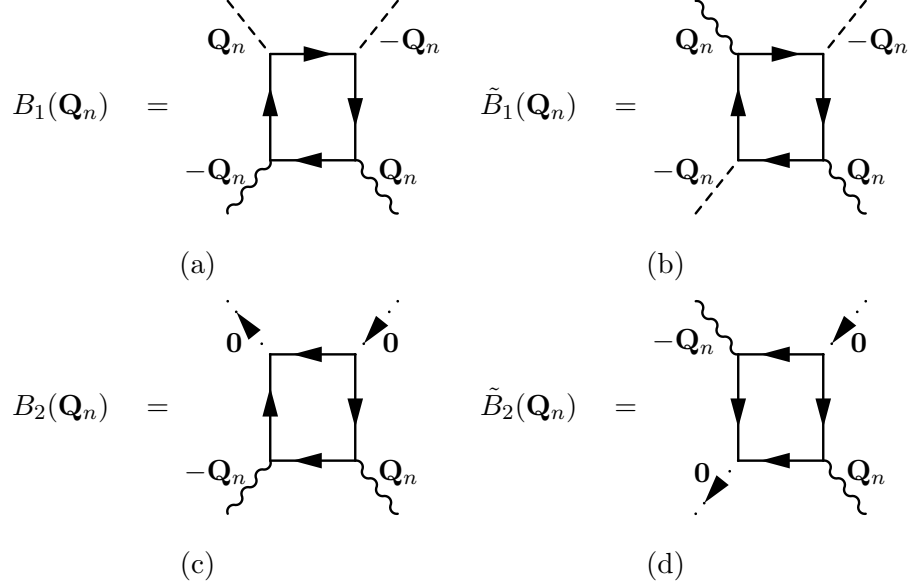


FIG. 6: Box diagrams yielding the lowest-order couplings between phonons and BDW as well as pairing fluctuations. Wavy lines represent phonons, dashed and dotted lines BDW and dSC fluctuations, respectively.

such as those near $\mathbf{q} = 0$, is qualitatively similar to that of the unsoftened mode in Fig. 5. In Fig. 5b, we show the time-averaged Raman displacement after long excitation times. The maximum of the time-averaged Raman displacement after excitation pulses behaves in a qualitatively similar way. It is interesting to note that a similar threshold behavior is also observed in experiments [3].

IV. COUPLING OF PHONONS TO BOND-DENSITY WAVE AND PAIRING FLUCTUATIONS

We now investigate the effect of the proposed strongly driven Raman modes near \mathbf{Q}_n on BDW and dSC fluctuations in the pseudogap phase. To do this, we integrate out the fermions, producing corrections to the effective action of the phenomenological model describing the competition of these order parameters. The simplest corrections are given by the “box” diagrams [42] shown in Fig. 6. We consider only diagrams where the fermions are close to the Fermi surface throughout all stages of the scattering process, as these are expected to be most relevant at low temperatures. The resulting mass renormalization for

BDW and dSC fluctuations reads

$$\delta S_{\text{cl}} = T \int d^2\mathbf{x} \sum_{n=x,y} \langle\langle \varphi(\mathbf{Q}_n)^2 \rangle\rangle \left[B_1(\mathbf{Q}_n) |\Phi_n|^2 + \tilde{B}_1(\mathbf{Q}_n) \text{Re}[\Phi_n^2] \right. \\ \left. + \left(B_2(\mathbf{Q}_n) + \tilde{B}_2(\mathbf{Q}_n) \right) |\Psi|^2 \right], \quad (29)$$

where the $\langle\langle \rangle\rangle$ denotes time-averaging over an oscillation cycle. $\langle\langle \varphi(\mathbf{Q}_n)^2 \rangle\rangle$ depends on A_{IR} as shown in Fig. 5b. For simplicity we ignore specifics of the transient behavior in this work. We are also making the assumption that only the low-momentum modes of the NLSM are important, and their mass renormalization is given by that of the zero modes. The box integrals are then given by

$$B_1(\mathbf{Q}_n) = \tilde{B}_1(\mathbf{Q}_n) = \\ \lambda_{\text{BDW}}^2 \lambda_{\text{ph}}^2 \int \frac{d^2\mathbf{k}}{(2\pi)^2} T \sum_{\omega_n} \sum_{\alpha_{1-4}=\pm} \frac{Z_{\mathbf{k}}^{\alpha_1} Z_{\mathbf{k}+\mathbf{Q}_n}^{\alpha_2} Z_{\mathbf{k}}^{\alpha_3} Z_{\mathbf{k}+\mathbf{Q}_n}^{\alpha_4} g_d(\mathbf{k} + \mathbf{Q}_n/2)^2 g_{\text{ph}}(\mathbf{Q}_n)^2}{(i\omega_n - E_{\mathbf{k}}^{\alpha_1})(i\omega_n - E_{\mathbf{k}+\mathbf{Q}_n}^{\alpha_2})(i\omega_n - E_{\mathbf{k}}^{\alpha_3})(i\omega_n - E_{\mathbf{k}+\mathbf{Q}_n}^{\alpha_4})}, \quad (30)$$

$$B_2(\mathbf{Q}_n) = -\lambda_{\text{dSC}}^2 \lambda_{\text{ph}}^2 \times \\ \times \int \frac{d^2\mathbf{k}}{(2\pi)^2} T \sum_{\omega_n} \sum_{\alpha_{1-4}=\pm} \frac{Z_{\mathbf{k}}^{\alpha_1} Z_{\mathbf{k}+\mathbf{Q}_n}^{\alpha_2} Z_{\mathbf{k}+\mathbf{Q}_n}^{\alpha_3} Z_{\mathbf{k}+\mathbf{Q}_n}^{\alpha_4} g_d(\mathbf{k} + \mathbf{Q}_n)^2 g_{\text{ph}}(\mathbf{Q}_n)^2}{(i\omega_n - E_{\mathbf{k}}^{\alpha_1})(i\omega_n - E_{\mathbf{k}+\mathbf{Q}_n}^{\alpha_2})(i\omega_n + E_{\mathbf{k}+\mathbf{Q}_n}^{\alpha_3})(i\omega_n - E_{\mathbf{k}+\mathbf{Q}_n}^{\alpha_4})}, \quad (31)$$

$$\tilde{B}_2(\mathbf{Q}_n) = \lambda_{\text{dSC}}^2 \lambda_{\text{ph}}^2 \int \frac{d^2\mathbf{k}}{(2\pi)^2} T \sum_{\omega_n} \sum_{\alpha_{1-4}=\pm} \frac{Z_{\mathbf{k}}^{\alpha_1} Z_{\mathbf{k}+\mathbf{Q}_n}^{\alpha_2} Z_{\mathbf{k}+\mathbf{Q}_n}^{\alpha_3} Z_{\mathbf{k}}^{\alpha_4} g_d(\mathbf{k}) g_d(\mathbf{k} + \mathbf{Q}_n) g_{\text{ph}}(\mathbf{Q}_n)^2}{(i\omega_n - E_{\mathbf{k}}^{\alpha_1})(i\omega_n - E_{\mathbf{k}+\mathbf{Q}_n}^{\alpha_2})(i\omega_n + E_{\mathbf{k}+\mathbf{Q}_n}^{\alpha_3})(i\omega_n + E_{\mathbf{k}}^{\alpha_4})}, \quad (32)$$

where we have exploited the evenness of certain quantities to simplify the expressions. Note that if the contribution to these diagrams comes mostly from “hot” regions of the Fermi surface that are nested by \mathbf{Q}_n , where $E_{\mathbf{k}+\mathbf{Q}_n}^{\pm} \approx -E_{\mathbf{k}}^{\pm}$, $Z_{\mathbf{k}+\mathbf{Q}_n}^{\pm} \approx Z_{\mathbf{k}}^{\pm}$, and $g_d(\mathbf{k} + \mathbf{Q}_n) \approx g_d(\mathbf{k})$, \mathbf{Q}_n , B_2 and \tilde{B}_2 will nearly cancel.

Let us start by deriving the low-temperature scaling of these diagrams. At very low temperatures, we can set $\alpha_{1-4} = -$. The corrections to the box integrals from the terms excluded by doing this are at most $O(T/\Delta)$, where $\Delta \sim E_{\mathbf{k}}^+ - E_{\mathbf{k}}^- \gg T$. At low temperatures, the integrands of the box diagrams are strongly peaked at the hot regions near the tips of the hole pockets. By making a gradient expansion of the dispersion at the pocket tips connected by for example \mathbf{Q}_y , which yields $E_{\mathbf{k}}^- \sim -vk_y + \kappa k_x^2$ and $E_{\mathbf{k}+\mathbf{Q}_y}^- \sim vk_y + \kappa k_x^2$ (see Fig. 2), we can estimate the low-temperature behavior of the diagrams. The form factors

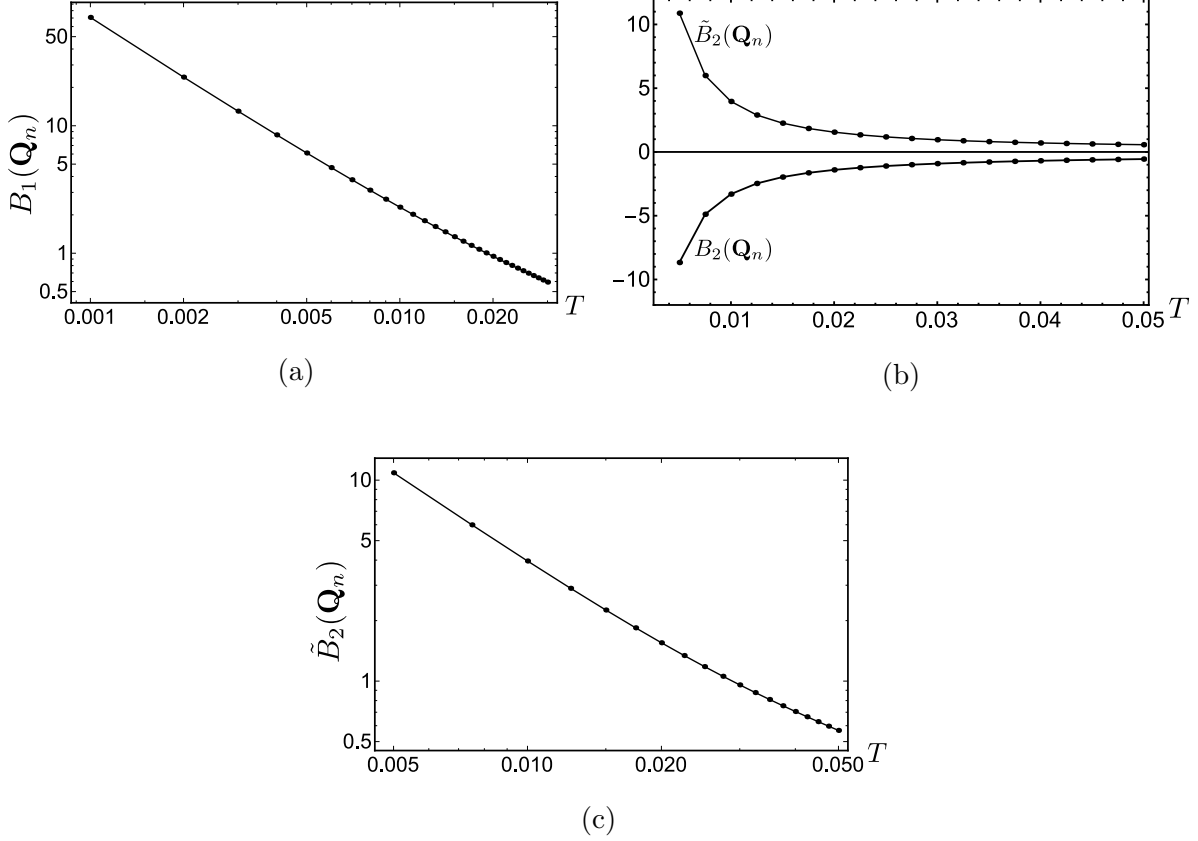


FIG. 7: Temperature dependence of box diagrams: (a) $B_1(\mathbf{Q}_n)$, (b) $B_2(\mathbf{Q}_n)$ and $\tilde{B}_2(\mathbf{Q}_n)$, (c) $\tilde{B}_2(\mathbf{Q}_n)$. Note that $B_2(\mathbf{Q}_n) \approx -\tilde{B}_2(\mathbf{Q}_n)$. We used momentum-independent electron-phonon vertices for simplicity and set $\lambda_{\text{BDW}} = \lambda_{\text{dSC}} = \lambda_{\text{ph}} = 1$ for the purpose of visualization.

and quasiparticle residues are slowly varying near the tips and may thus be approximated by the value at the tips of the pockets. The box integrals still converge in this limit, and a simple rescaling of momenta, $k_y \rightarrow Tk_y$ and $k_x \rightarrow \sqrt{T}k_x$, then yields $B_1, B_2, \tilde{B}_2 \sim T^{-3/2}$. The corrections to the mass terms in the effective action hence scale as $T^{-1/2}$. Also, since particle-hole symmetry holds to linear order in \mathbf{k} , there is a near cancellation between B_2 and \tilde{B}_2 . These statements are confirmed by numerical evaluation of the diagrams without these restrictions, as shown in Fig. 7. The temperature dependence of the renormalized vertices or the corrections with d -wave form factors do not significantly affect the scaling and the cancellation between B_2 and \tilde{B}_2 . We find $B_1(\mathbf{Q}_n) > 0$ and $B_2(\mathbf{Q}_n) \approx -\tilde{B}_2(\mathbf{Q}_n) < 0$.

The leading corrections to the effective action thus simplify to

$$\delta S_{\text{cl}} \approx T \int d^2\mathbf{x} \sum_{n=x,y} \langle\langle \varphi(\mathbf{Q}_n)^2 \rangle\rangle B_1(\mathbf{Q}_n) \text{Re}[\Phi_n]^2, \quad (33)$$

yielding a mass enhancement for BDW fluctuations along the $\text{Re}[\Phi_n]$ directions (*i. e.* $m^2 \rightarrow m'^2 = m^2 + \frac{2T}{\rho_s} \langle\langle \varphi(\mathbf{Q}_n)^2 \rangle\rangle B_1(\mathbf{Q}_n)$). In order to demonstrate that this is indeed favorable for superconductivity, we assume that the time-averaged behavior is equivalent to an effective equilibrium model for which we can compute the enhancement of T_c . This is certainly only indicative for the non-equilibrium situation, and should not be taken as a serious quantitative estimate of the strength of any transient superconducting state. True transient superconducting behavior can only be understood by solving the full time-dependent problem and studying the behavior of the superfluid density, which is beyond the scope of this work. Note that within our approximations, the coupling of order parameters to driven phonons acts as a parameter quench for the non-linear sigma model. The results of Fu *et al.* [24] then suggest that the qualitative trends in the time-averaged results carry over to a solution of the equations of motion. The T_c enhancement is computed by condensing one component of the dSC order parameter and neglecting fluctuations that would vanish in a large- N limit, as done in Ref. 43. The gap equation reads

$$\Psi_0^2 = 1 - \frac{T}{3\rho_s} \left(\int^\Lambda \frac{d^2\mathbf{k}}{(2\pi)^2} \frac{1}{k^2} + \int^\Lambda \frac{d^2\mathbf{k}}{(2\pi)^2} \frac{1}{\eta k^2 + m^2} + \int^\Lambda \frac{d^2\mathbf{k}}{(2\pi)^2} \frac{1}{\eta k^2 + m'^2} \right) = 1 - \frac{T}{T_c}. \quad (34)$$

This can be regulated and the T_c enhancement computed by differentiating and re-integrating with respect to m'^2 , yielding

$$T_c = \frac{T_c^{(0)}}{1 - \frac{T_c^{(0)}}{12\pi\rho_s\eta} \ln\left(\frac{m'^2}{m^2}\right)}. \quad (35)$$

The logarithm suggests that the enhancement of superconductivity is a modest effect. Nevertheless, it is a correction in the correct direction, which is basically what we wanted to demonstrate.

In the appendix, we present further results for the momentum dependence of the box diagrams (Appendix A) and for the influence of the geometry of the Fermi surface (Appendix B). The sign structure of the box diagrams implies that it would be detrimental for the proposed mechanism of enhancing superconductivity if phonons with other momenta than the BDW wave vector are strongly driven. Moreover, BDW with axial wave vectors cannot be efficiently melted in a system with a large Fermi surface. However, for BDW with diagonal wave vectors conclusions similar to those in this section hold.

V. DISCUSSION AND CONCLUSIONS

In summary, we proposed a theory for light-induced superconductivity and phonon renormalization in slightly underdoped cuprates below the onset temperature for BDW fluctuations. We described the competition between superconductivity and BDW fluctuations by a phenomenological model and studied how the interplay between the two orders is influenced by externally driven phonons. At an incipient BDW instability in a system with a small Fermi surface, as in a fractionalized Fermi liquid, the electron-phonon vertex is strongly enhanced, which leads to a significant softening of the phonon dispersion at the BDW wave vector. It is expected that the softening due to BDW fluctuations is also accompanied by a strongly enhanced phonon linewidth, the latter being observed in experiment [30].

The phonon softening at the BDW wave vector entails large phonon oscillations or displacements when the system is sufficiently strongly driven with light. Due to the strong coupling between phonons at the BDW wave vector and BDW fluctuations, this leads to an efficient melting of BDW correlations by renormalizing the mass of BDW fluctuations. The coupling between phonons and Cooper pairs is significantly smaller because certain quartic couplings between them nearly cancel. This asymmetry regarding the mass renormalization for collective excitations tips the balance between competing orders towards pairing correlations when the system is stimulated with light. A time-averaged approximation for the phenomenological model of competing orders yields an enhancement of T_c , which may give rise to a transient superconducting state in a dynamical treatment. The latter is, however, beyond the scope of the present work.

The proposed mechanism is applicable only below the onset temperature of BDW fluctuations and cannot explain the transient superconducting state that is found up to room temperature. Our theory for phonon renormalizations could be tested by repeating the experiments by Le Tacon *et al.* [30] in a magnetic field slightly below the zero-field equilibrium T_c . Suppressing superconductivity should make BDW fluctuations more critical and yield a stronger renormalization of the phonon dispersion and linewidth, leading to a continuation of the trends that are found above T_c . Another test of our theory would be possible by measuring the momentum-space power spectrum of the driven phonons in the transient superconducting state. According to our theory, the (Raman) phonons at the BDW wavevector should be excited much more strongly than those at other wavevectors. The proposed

mechanism for enhanced superconductivity could presumably work collaboratively with the mechanism involving interlayer hopping suggested by Raines *et al.* [15], which would enhance the effect.

This work also constitutes a first step towards an understanding of controlling competing order parameters by driving phonons with light. A theory similar to the one suggested in this work could be applicable to stripe ordered Lanthanum-based cuprates [6], in which strong phonon softening is also observed [44]. The similarities regarding two-dimensional incommensurate charge correlations, anomalous strength of phonon softening and role of anharmonicity effects in YBCO and NbSe₂ [45] provoke the question whether it would also be possible to melt CDW order by excitation of phonons with light in the latter material.

ACKNOWLEDGMENTS

We acknowledge valuable discussions with D. Chowdhury, S. Kaiser and S. Sachdev. This research was supported by the NSF under Grant DMR-1360789 and the German National Academy of Sciences Leopoldina through grant LPDS 2014-13.

Appendix A: Other Phonon Wavevectors

In this appendix we present results for the momentum dependence of quartic couplings of order parameters and certain other phonon modes, although we deduced that these are not as strongly driven as the modes near \mathbf{Q}_n . For simplicity we approximate the electron-phonon vertex by a momentum-independent one (we are only interested in the qualitative behavior of the box integrals across the Brillouin zone). Then the dependence on the phonon momentum \mathbf{q} of the box diagram contributing to the dSC mass renormalization ($B_2(\mathbf{q}) + \tilde{B}_2(\mathbf{q})$) is shown in Fig. 8a. It is close to zero or even negative, except when \mathbf{q} is near zero, where it is strongly positive due to nesting all over the Fermi surface. Hence, it is essential that the phonon modes near $\mathbf{q} = 0$ are not strongly driven for the proposed mechanism for light-induced superconductivity to work. This can be tested in an experiment by measuring the momentum-space power spectrum of the driven phonons.

Figure 8b shows $B_1(\mathbf{q})$ for arbitrary phonon momenta \mathbf{q} . There are no regions where it is strongly negative. Figure 9 shows the other scattering processes that couple BDW

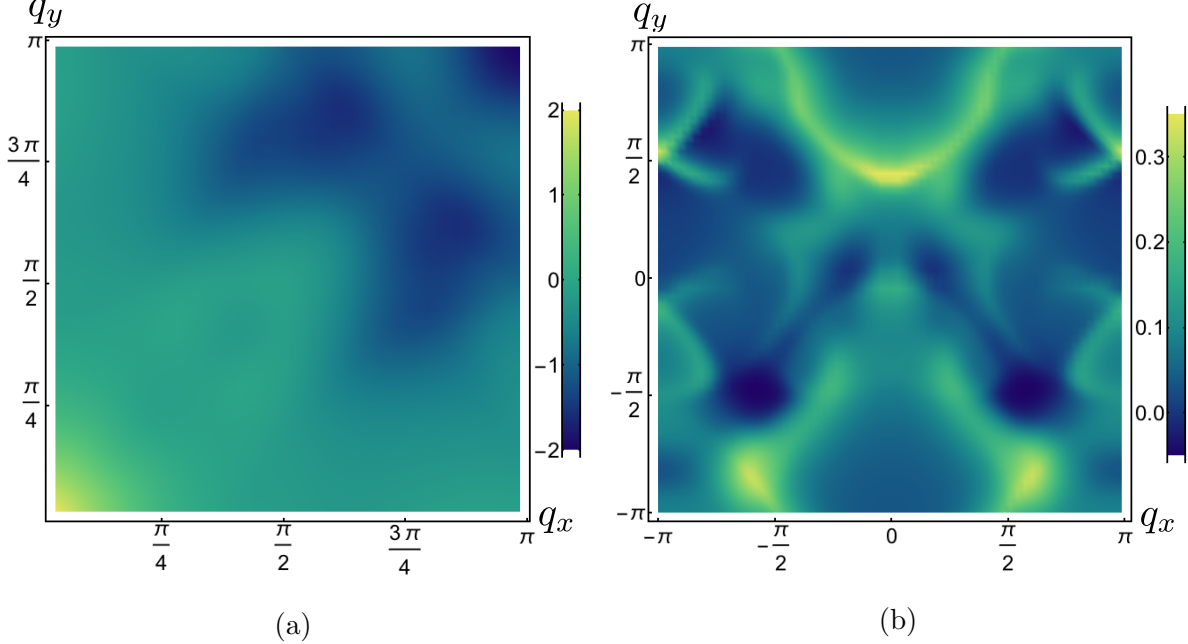


FIG. 8: (Color online) Momentum dependence of box diagrams: (a) $B_2(\mathbf{q}) + \tilde{B}_2(\mathbf{q})$ and (b) $B_1(\mathbf{q})$. The temperature is $T = 0.05$ in both plots. We have again used momentum-independent electron-phonon vertices and set $\lambda_{\text{BDW}} = \lambda_{\text{dSC}} = \lambda_{\text{ph}} = 1$ for the purpose of visualization.

fluctuations to certain phonons. The first diagram, coupling the BDW to the phonon with $\mathbf{q} = \mathbf{0}$, is equivalent to $B_1(\mathbf{Q}_n)$ and is positive. The second and third diagrams are equal to each other and are also positive. All of them scale as $T^{-3/2}$ since they mainly involve the pocket tips.

Appendix B: Large Fermi Surface

In this appendix we discuss the influence of the Fermi surface geometry on the coupling between phonons and order parameter fluctuations. For the large Fermi surface (Fig 2b), the leading BDW instabilities are at the diagonal wavevectors $(Q, \pm Q)$ [27, 46]. Consequently the phonon softening is strongest at these wavevectors, and our mechanism highlights the coupling of phonons at these wavevectors to the order parameters. The box diagrams coupling to the order parameters are easily computed in the linearized hot-spot approximation

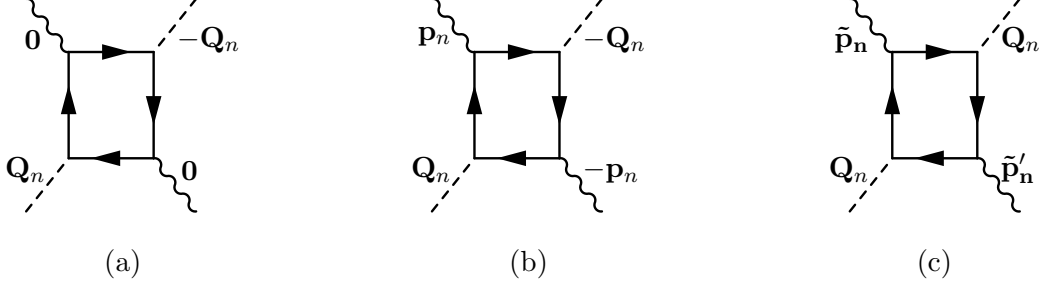


FIG. 9: Some additional box diagrams yielding lowest-order couplings between phonons and BDW fluctuations at various other wave vectors. The wavevector \mathbf{p}_y connects the tips of the pockets at (k_x, k_y) and $(-k_x, k_y)$, $\tilde{\mathbf{p}}_y = \mathbf{p}_y - \mathbf{Q}_y$, $\tilde{\mathbf{p}}'_y = -\mathbf{p}_y - \mathbf{Q}_y$, and likewise for $y \leftrightarrow x$.

and are given by (dropping coupling constants and phonon form factors)

$$B_1(Q, \pm Q) = \tilde{B}_1(Q, \pm Q) \sim \int \frac{d^2\mathbf{k}}{(2\pi)^2} T \sum_{\omega_n} \frac{1}{(i\omega_n - \mathbf{v} \cdot \mathbf{k})^2} \frac{1}{(i\omega_n + \mathbf{v} \cdot \mathbf{k})^2} = \frac{7\Lambda_{\parallel}\zeta(3)}{32\pi^4 T^2 |\mathbf{v}|}, \quad (\text{B1})$$

$$B_2(Q, \pm Q) = -\tilde{B}_2(Q, \pm Q) = -B_1(Q, \pm Q), \quad (\text{B2})$$

where \mathbf{v} is the Fermi velocity at one hot spot. Note the exact cancellation between B_2 and \tilde{B}_2 . The rest of the story is exactly the same and (Q, Q) -BDW order could be melted by driving the phonon with the same wavevector.

If the axial wavevectors \mathbf{Q}_n (which is not the leading instability) are used, the box diagrams yield

$$B_1(\mathbf{Q}_n) = \tilde{B}_1(\mathbf{Q}_n) \sim \int \frac{d^2\mathbf{k}}{(2\pi)^2} T \sum_{\omega_n} \frac{1}{(i\omega_n - \mathbf{v}_1 \cdot \mathbf{k})^2} \frac{1}{(i\omega_n - \mathbf{v}_2 \cdot \mathbf{k})^2} = 0, \quad (\text{B3})$$

$$B_2(\mathbf{Q}_n) \sim - \int \frac{d^2\mathbf{k}}{(2\pi)^2} T \sum_{\omega_n} \frac{1}{(i\omega_n - \mathbf{v}_1 \cdot \mathbf{k})^2} \frac{1}{(i\omega_n + \mathbf{v}_1 \cdot \mathbf{k})} \frac{1}{(i\omega_n - \mathbf{v}_2 \cdot \mathbf{k})} = -\frac{1}{32|\mathbf{v}_1 \times \mathbf{v}_2|T}, \quad (\text{B4})$$

$$\begin{aligned} \tilde{B}_2(\mathbf{Q}_n) &\sim \int \frac{d^2\mathbf{k}}{(2\pi)^2} T \sum_{\omega_n} \frac{1}{(i\omega_n - \mathbf{v}_1 \cdot \mathbf{k})} \frac{1}{(i\omega_n + \mathbf{v}_1 \cdot \mathbf{k})} \frac{1}{(i\omega_n + \mathbf{v}_2 \cdot \mathbf{k})} \frac{1}{(i\omega_n - \mathbf{v}_2 \cdot \mathbf{k})} \\ &= \frac{1}{16|\mathbf{v}_1 \times \mathbf{v}_2|T}, \end{aligned} \quad (\text{B5})$$

where \mathbf{v}_1 and \mathbf{v}_2 are the Fermi velocities at the hot spots connected by \mathbf{Q}_n . Hence the proposed mechanism would not work because B_1 vanishes and melting of BDW correlations with wavevector \mathbf{Q}_n is not possible by driving phonons. There is also no cancellation between

B_2 and \tilde{B}_2 in this case. Having a sizable coupling between BDW fluctuations and phonons at wavevector \mathbf{Q}_n thus requires a small Fermi surface.

-
- [1] R. I. Tobey, D. Prabhakaran, A. T. Boothroyd, and A. Cavalleri, “Ultrafast electronic phase transition in $\text{La}_{1/2}\text{Sr}_{3/2}\text{MnO}_4$ by coherent vibrational excitation: Evidence for nonthermal melting of orbital order,” *Phys. Rev. Lett.* **101**, 197404 (2008).
- [2] M. Först, R. I. Tobey, S. Wall, H. Bromberger, V. Khanna, A. L. Cavalieri, Y.-D. Chuang, W. S. Lee, R. Moore, W. F. Schlotter, J. J. Turner, O. Krupin, M. Trigo, H. Zheng, J. F. Mitchell, S. S. Dhesi, J. P. Hill, and A. Cavalleri, “Driving magnetic order in a manganite by ultrafast lattice excitation,” *Phys. Rev. B* **84**, 241104 (2011), [arXiv:1105.3866 \[cond-mat.str-el\]](#).
- [3] S. Kaiser, C. R. Hunt, D. Nicoletti, W. Hu, I. Gierz, H. Y. Liu, M. Le Tacon, T. Loew, D. Haug, B. Keimer, and A. Cavalleri, “Optically induced coherent transport far above T_c in underdoped $\text{YBa}_2\text{Cu}_3\text{O}_{6+\delta}$,” *Phys. Rev. B* **89**, 184516 (2014), [arXiv:1205.4661 \[cond-mat.supr-con\]](#).
- [4] D. Fausti, R. I. Tobey, N. Dean, S. Kaiser, A. Dienst, M. C. Hoffmann, S. Pyon, T. Takayama, H. Takagi, and A. Cavalleri, “Light-induced superconductivity in a stripe-ordered cuprate,” *Science* **331**, 189–191 (2011).
- [5] E. Casandruc, D. Nicoletti, S. Rajasekaran, Y. Laplace, V. Khanna, G. D. Gu, J. P. Hill, and A. Cavalleri, “Wavelength-dependent optical enhancement of superconducting interlayer coupling in $\text{La}_{1.885}\text{Ba}_{0.115}\text{CuO}_4$,” *Phys. Rev. B* **91**, 174502 (2015), [arXiv:1505.02167 \[cond-mat.supr-con\]](#).
- [6] C. R. Hunt, D. Nicoletti, S. Kaiser, T. Takayama, H. Takagi, and A. Cavalleri, “Two distinct kinetic regimes for the relaxation of light-induced superconductivity in $\text{La}_{1.675}\text{Eu}_{0.2}\text{Sr}_{0.125}\text{CuO}_4$,” *Phys. Rev. B* **91**, 020505 (2015), [arXiv:1502.03028 \[cond-mat.supr-con\]](#).
- [7] M. Först, R. I. Tobey, H. Bromberger, S. B. Wilkins, V. Khanna, A. D. Caviglia, Y.-D. Chuang, W. S. Lee, W. F. Schlotter, J. J. Turner, M. P. Minitti, O. Krupin, Z. J. Xu, J. S. Wen, G. D. Gu, S. S. Dhesi, A. Cavalleri, and J. P. Hill, “Melting of charge stripes in vibrationally driven $\text{La}_{1.875}\text{Ba}_{0.125}\text{CuO}_4$: Assessing the respective roles of electronic and lattice order in frustrated

- superconductors,” *Phys. Rev. Lett.* **112**, 157002 (2014), [arXiv:1406.2483 \[cond-mat.supr-con\]](#).
- [8] M. Först, A. Frano, S. Kaiser, R. Mankowsky, C. R. Hunt, J. J. Turner, G. L. Dakovski, M. P. Minitti, J. Robinson, T. Loew, M. Le Tacon, B. Keimer, J. P. Hill, A. Cavalleri, and S. S. Dhesi, “Femtosecond x rays link melting of charge-density wave correlations and light-enhanced coherent transport in $\text{YBa}_2\text{Cu}_3\text{O}_{6.6}$,” *Phys. Rev. B* **90**, 184514 (2014), [arXiv:1502.05343 \[cond-mat.supr-con\]](#).
- [9] W. Hu, S. Kaiser, D. Nicoletti, C. R. Hunt, I. Gierz, M. C. Hoffmann, M. Le Tacon, T. Loew, B. Keimer, and A. Cavalleri, “Optically enhanced coherent transport in $\text{YBa}_2\text{Cu}_3\text{O}_{6.5}$ by ultrafast redistribution of interlayer coupling,” *Nat. Mater.* **13**, 705–711 (2014), [arXiv:1308.3204 \[cond-mat.supr-con\]](#).
- [10] R. Mankowsky, A. Subedi, M. Först, S. O. Mariager, M. Chollet, H. T. Lemke, J. S. Robinson, J. M. Glownia, M. P. Minitti, A. Frano, M. Fechner, N. A. Spaldin, T. Loew, B. Keimer, A. Georges, and A. Cavalleri, “Nonlinear lattice dynamics as a basis for enhanced superconductivity in $\text{YBa}_2\text{Cu}_3\text{O}_{6.5}$,” *Nature* **516**, 71–73 (2014), [arXiv:1405.2266 \[cond-mat.supr-con\]](#).
- [11] R. Mankowsky, M. Först, T. Loew, J. Porras, B. Keimer, and A. Cavalleri, “Coherent modulation of the $\text{YBa}_2\text{Cu}_3\text{O}_{6+x}$ atomic structure by displacive stimulated ionic Raman scattering,” *Phys. Rev. B* **91**, 094308 (2015), [arXiv:1505.06127 \[cond-mat.supr-con\]](#).
- [12] A. Dubroka, M. Rössle, K. W. Kim, V. K. Malik, D. Munzar, D. N. Basov, A. A. Schafgans, S. J. Moon, C. T. Lin, D. Haug, V. Hinkov, B. Keimer, Th. Wolf, J. G. Storey, J. L. Tallon, and C. Bernhard, “Evidence of a precursor superconducting phase at temperatures as high as 180 K in $\text{R}\text{Ba}_2\text{Cu}_3\text{O}_{7-\delta}$ ($\text{R} = \text{Y}, \text{Gd}, \text{Eu}$) superconducting crystals from infrared spectroscopy,” *Phys. Rev. Lett.* **106**, 047006 (2011), [arXiv:1009.2925 \[cond-mat.supr-con\]](#).
- [13] R. Höppner, B. Zhu, T. Rexin, A. Cavalleri, and L. Mathey, “Redistribution of phase fluctuations in a periodically driven cuprate superconductor,” *Phys. Rev. B* **91**, 104507 (2015), [arXiv:1406.3609 \[cond-mat.supr-con\]](#).
- [14] S. J. Denny, S. R. Clark, Y. Laplace, A. Cavalleri, and D. Jaksch, “Proposed parametric cooling of bilayer cuprate superconductors by terahertz excitation,” *Phys. Rev. Lett.* **114**, 137001 (2015), [arXiv:1411.3258 \[cond-mat.supr-con\]](#).
- [15] Z. M. Raines, V. Stanev, and V. M. Galitski, “Enhancement of superconductivity via periodic modulation in a three-dimensional model of cuprates,” *Phys. Rev. B* **91**, 184506 (2015), [arXiv:1501.06922 \[cond-mat.supr-con\]](#).

- [16] A. Subedi, A. Cavalleri, and A. Georges, “Theory of nonlinear phononics for coherent light control of solids,” *Phys. Rev. B* **89**, 220301 (2014), [arXiv:1311.0544 \[cond-mat.str-el\]](#).
- [17] G.M. Eliashberg, “Film superconductivity stimulated by a high-frequency field,” *JETP Lett.* **11**, 114 (1970).
- [18] B.I. Ivlev and G.M. Eliashberg, “Influence of nonequilibrium excitations on the properties of superconducting films in a high-frequency field,” *JETP Lett.* **13**, 333 (1971).
- [19] G. Ghiringhelli, M. Le Tacon, M. Minola, S. Blanco-Canosa, C. Mazzoli, N. B. Brookes, G. M. De Luca, A. Frano, D. G. Hawthorn, F. He, T. Loew, M. Moretti Sala, D. C. Peets, M. Salluzzo, E. Schierle, R. Sutarto, G. A. Sawatzky, E. Weschke, B. Keimer, and L. Braicovich, “Long-range incommensurate charge fluctuations in $(Y, Nd)Ba_2Cu_3O_{6+x}$,” *Science* **337**, 821–825 (2012), [arXiv:1207.0915 \[cond-mat.str-el\]](#).
- [20] J. Chang, E. Blackburn, A. T. Holmes, N. B. Christensen, J. Larsen, J. Mesot, Ruixing Liang, D. A. Bonn, W. N. Hardy, A. Watenphul, M. v. Zimmermann, E. M. Forgan, and S. M. Hayden, “Direct observation of competition between superconductivity and charge density wave order in $YBa_2Cu_3O_{6.67}$,” *Nat. Phys.* **8**, 871–876 (2012), [arXiv:1206.4333 \[cond-mat.supr-con\]](#).
- [21] S. Blanco-Canosa, A. Frano, T. Loew, Y. Lu, J. Porras, G. Ghiringhelli, M. Minola, C. Mazzoli, L. Braicovich, E. Schierle, E. Weschke, M. Le Tacon, and B. Keimer, “Momentum-dependent charge correlations in $YBa_2Cu_3O_{6+\delta}$ superconductors probed by resonant x-ray scattering: Evidence for three competing phases,” *Phys. Rev. Lett.* **110**, 187001 (2013), [arXiv:1212.5580 \[cond-mat.supr-con\]](#).
- [22] H. Meier, M. Einenkel, C. Pépin, and K. B. Efetov, “Effect of magnetic field on the competition between superconductivity and charge order below the pseudogap state,” *Phys. Rev. B* **88**, 020506 (2013), [arXiv:1306.6871 \[cond-mat.str-el\]](#).
- [23] L. E. Hayward, D. G. Hawthorn, R. G. Melko, and S. Sachdev, “Angular fluctuations of a multicomponent order describe the pseudogap of $YBa_2Cu_3O_{6+x}$,” *Science* **343**, 1336–1339 (2014), [arXiv:1309.6639 \[cond-mat.supr-con\]](#).
- [24] W. Fu, L.-Y. Hung, and S. Sachdev, “Quantum quenches and competing orders,” *Phys. Rev. B* **90**, 024506 (2014), [arXiv:1401.7674 \[cond-mat.supr-con\]](#).
- [25] T. Senthil, S. Sachdev, and M. Vojta, “Fractionalized Fermi liquids,” *Phys. Rev. Lett.* **90**, 216403 (2003), [arXiv:cond-mat/0209144](#).

- [26] T. Senthil, M. Vojta, and S. Sachdev, “Weak magnetism and non-Fermi liquids near heavy-fermion critical points,” *Phys. Rev. B* **69**, 035111 (2004), [arXiv:cond-mat/0305193](#).
- [27] D. Chowdhury and S. Sachdev, “Density-wave instabilities of fractionalized Fermi liquids,” *Phys. Rev. B* **90**, 245136 (2014), [arXiv:1409.5430 \[cond-mat.str-el\]](#).
- [28] R. Comin, A. Frano, M. M. Yee, Y. Yoshida, H. Eisaki, E. Schierle, E. Weschke, R. Sutarto, F. He, A. Soumyanarayanan, Yang He, M. Le Tacon, I. S. Elfimov, Jennifer E. Hoffman, G. A. Sawatzky, B. Keimer, and A. Damascelli, “Charge order driven by Fermi-arc instability in $\text{Bi}_2\text{Sr}_{2-x}\text{La}_x\text{CuO}_{6+\delta}$,” *Science* **343**, 390–392 (2014), [arXiv:1312.1343 \[cond-mat.supr-con\]](#).
- [29] M. Raichle, D. Reznik, D. Lamago, R. Heid, Y. Li, M. Bakr, C. Ulrich, V. Hinkov, K. Hradil, C. T. Lin, and B. Keimer, “Highly anisotropic anomaly in the dispersion of the copper-oxygen bond-bending phonon in superconducting $\text{YBa}_2\text{Cu}_3\text{O}_7$ from inelastic neutron scattering,” *Phys. Rev. Lett.* **107**, 177004 (2011), [arXiv:1109.5511 \[cond-mat.str-el\]](#).
- [30] M. Le Tacon, A. Bosak, S. M. Souliou, G. Dellea, T. Loew, R. Heid, K-P. Bohnen, G. Ghiringhelli, M. Krisch, and B. Keimer, “Inelastic x-ray scattering in $\text{YBa}_2\text{Cu}_3\text{O}_{6.6}$ reveals giant phonon anomalies and elastic central peak due to charge-density-wave formation,” *Nat. Phys.* **10**, 52–58 (2014), [arXiv:1307.1673 \[cond-mat.supr-con\]](#).
- [31] E. Blackburn, J. Chang, A. H. Said, B. M. Leu, Ruixing Liang, D. A. Bonn, W. N. Hardy, E. M. Forgan, and S. M. Hayden, “Inelastic x-ray study of phonon broadening and charge-density wave formation in ortho-ii-ordered $\text{YBa}_2\text{Cu}_3\text{O}_{6.54}$,” *Phys. Rev. B* **88**, 054506 (2013), [arXiv:1307.1672 \[cond-mat.supr-con\]](#).
- [32] Y. Qi and S. Sachdev, “Effective theory of fermi pockets in fluctuating antiferromagnets,” *Phys. Rev. B* **81**, 115129 (2010), [arXiv:0912.0943 \[cond-mat.str-el\]](#).
- [33] D. Chowdhury and S. Sachdev, “The enigma of the pseudogap phase of the cuprate superconductors,” ArXiv e-prints (2015), [arXiv:1501.00002 \[cond-mat.str-el\]](#).
- [34] A. Allais, D. Chowdhury, and S. Sachdev, “Connecting high-field quantum oscillations to zero-field electron spectral functions in the underdoped cuprates,” *Nat. Commun.* **5**, 6771 (2014), [arXiv:1406.0503 \[cond-mat.str-el\]](#).
- [35] Y. Wang and A. Chubukov, “Charge-density-wave order with momentum $(2Q, 0)$ and $(0, 2Q)$ within the spin-fermion model: Continuous and discrete symmetry breaking, preemptive composite order, and relation to pseudogap in hole-doped cuprates,” *Phys. Rev. B* **90**, 035149 (2014), [arXiv:1401.0712 \[cond-mat.str-el\]](#).

- [36] A. Allais, J. Bauer, and S. Sachdev, “Density wave instabilities in a correlated two-dimensional metal,” *Phys. Rev. B* **90**, 155114 (2014), [arXiv:1402.4807 \[cond-mat.str-el\]](#).
- [37] R. Comin, R. Sutarto, F. He, E. H. da Silva Neto, L. Chauviere, A. Frano, R. Liang, W. N. Hardy, D. A. Bonn, Y. Yoshida, H. Eisaki, A. J. Achkar, D. G. Hawthorn, B. Keimer, G. A. Sawatzky, and A. Damascelli, “Symmetry of charge order in cuprates,” *Nat. Mater.* **14**, 796–800 (2015), [arXiv:1402.5415 \[cond-mat.supr-con\]](#).
- [38] N. Bulut and D. J. Scalapino, “ $d_{x^2-y^2}$ symmetry and the pairing mechanism,” *Phys. Rev. B* **54**, 14971–14973 (1996), [arXiv:cond-mat/9609131](#).
- [39] M. Knap, M. Babadi, G. Refael, I. Martin, and E. Demler, “Dynamical Cooper pairing in non-equilibrium electron-phonon systems,” *ArXiv e-prints* (2015), [arXiv:1511.07874 \[cond-mat.supr-con\]](#).
- [40] M. Abramowitz and I. A. Stegun, *Handbook of mathematical functions: with formulas, graphs, and mathematical tables*, 55th ed. (Courier Corporation, 1964).
- [41] D. W. Jordan and P. Smith, *Nonlinear Ordinary Differential Equations*, 3rd ed., Oxford applied and engineering mathematics (Oxford University Press, 1999).
- [42] D. Chowdhury and S. Sachdev, “Feedback of superconducting fluctuations on charge order in the underdoped cuprates,” *Phys. Rev. B* **90**, 134516 (2014), [arXiv:1404.6532 \[cond-mat.str-el\]](#).
- [43] Subir Sachdev, *Quantum phase transitions* (Wiley Online Library, 2007).
- [44] D. Reznik, L. Pintschovius, M. Ito, S. Iikubo, M. Sato, H. Goka, M. Fujita, K. Yamada, G. D. Gu, and J. M. Tranquada, “Electron-phonon coupling reflecting dynamic charge inhomogeneity in copper oxide superconductors,” *Nature* **440**, 1170–1173 (2006), [arXiv:cond-mat/0512063](#).
- [45] M. Leroux, I. Errea, M. Le Tacon, S.-M. Souliou, G. Garbarino, L. Cario, A. Bosak, F. Mauri, M. Calandra, and P. Rodière, “Strong anharmonicity induces quantum melting of charge density wave in $2H\text{-NbSe}_2$ under pressure,” *Phys. Rev. B* **92**, 140303 (2015), [arXiv:1508.06463 \[cond-mat.supr-con\]](#).
- [46] S. Sachdev and R. La Placa, “Bond order in two-dimensional metals with antiferromagnetic exchange interactions,” *Phys. Rev. Lett.* **111**, 027202 (2013), [arXiv:1303.2114 \[cond-mat.supr-con\]](#).